

Fermi National Accelerator Laboratory

FERMILAB-Conf-96/049-E

CDF

Studies of Double-Sided Silicon Microstrip Detectors

**S.C. Seidel, N.L. Bruner, M.A. Frautsch, M.R. Hoferkamp and A. Patton
For the CDF Collaboration**

*The New Mexico Center for Particle Physics
The University of New Mexico
Albuquerque, New Mexico 87131*

*Fermi National Accelerator Laboratory
P.O. Box 500, Batavia, Illinois 60510*

March 1996

Published Proceedings *Second International Symposium on Development and Application of Semiconductor Tracking Detectors*, Hiroshima, Japan, October 10-13, 1995.



Disclaimer

This report was prepared as an account of work sponsored by an agency of the United States Government. Neither the United States Government nor any agency thereof, nor any of their employees, makes any warranty, express or implied, or assumes any legal liability or responsibility for the accuracy, completeness, or usefulness of any information, apparatus, product, or process disclosed, or represents that its use would not infringe privately owned rights. Reference herein to any specific commercial product, process, or service by trade name, trademark, manufacturer, or otherwise, does not necessarily constitute or imply its endorsement, recommendation, or favoring by the United States Government or any agency thereof. The views and opinions of authors expressed herein do not necessarily state or reflect those of the United States Government or any agency thereof.

STUDIES OF DOUBLE-SIDED SILICON MICROSTRIP DETECTORS

S. C. Seidel,* N. L. Bruner, M. A. Frautschi,[†]
M. R. Hoferkamp, A. Patton

The New Mexico Center for Particle Physics
The University of New Mexico
Albuquerque, NM 87131, USA

For the CDF Collaboration

18 December 1995

Abstract

The electrical characteristics of detectors manufactured by SINTEF/SI with a variety of geometrical and processing options have been investigated. The detectors' leakage current, depletion voltage, bias resistance, interstrip resistance, coupling capacitance, and coupling capacitor breakdown voltage were studied.

*Corresponding author.

[†]Present address: Department of Physics, Texas Tech University, Lubbock, TX 79409

Published Proceedings Second International Symposium on Development and Application of Semiconductor Tracking Detectors, Hiroshima, Japan, October 10-13, 1995

1 INTRODUCTION

Two batches of AC-coupled, double-sided silicon microstrip detectors which were manufactured by SINTEF/SI¹ have been electrically characterized. These detectors, prototypes for the SVX II [1], were manufactured in 8 varieties [2] whose distinguishing features are summarized in Table 1. In Table 1, “DM” indicates that the detector has double-metal readout on the n -side; “SM” indicates single metal readout on the n -side. The insulator used in the double-metal structure is polyimide. Intermediate strips are implant strips which have no aluminum readout strips associated with them. Strips on the n -side are isolated by a common p -stop. Bias voltage is applied through polysilicon resistors. The implants on the p - and n -sides are $10\mu\text{m}$ and $12\mu\text{m}$ wide, respectively. All detectors are $280\mu\text{m}$ thick.

Table 1: Features of the SINTEF/SI SVX II Prototype Detectors

Type	Inter- mediate Strips	Nominal Length (cm)	Nominal Width (cm)	p -side Implant Pitch (μm)	n -side Implant Pitch (μm)
A-SM	p -side	4.25	2.07	25	103
A-DM	p -side	4.25	2.07	25	103
B-SM	none	4.25	2.07	50	103
B-DM	none	4.25	2.07	50	103
C-SM	n -side	8.50	1.43	50	79
C-DM	n -side	8.50	1.43	50	79
D-SM	none	8.50	1.43	50	158
D-DM	none	8.50	1.43	50	158

The data sets in this paper are referred to as “Batch 1” (which numbers 24 detectors) and “Batch 2” (which includes 8 detectors). Detectors in both batches have their entire surface coated with silicon dioxide. The Batch 1 detectors have an additional coating of silicon nitride upon their entire surface, while on Batch 2 detectors, the silicon nitride is present only in the coupling capacitors [3]. The entire production run, including detectors known to be defective, was delivered for evaluation.

Characterization was conducted in order to select the strip geometry,

¹P. O. Box 124 Blindern, N-0314 Oslo, Norway.

passivation process, and n -side readout structure which are jointly optimized for maximum signal-to-noise ratio and resolution in a high radiation environment. The evaluation was also intended to monitor processing uniformity and conformance to specifications. Additional details about the detectors' geometries may be found in Tables 2 and 3 of Reference 4.

The techniques used to make these electrical measurements are explained in References 4 and 5. Additional information concerning the measurements may be found in Reference 6.

2 MEASUREMENTS

LEAKAGE CURRENT

Figure 1 is a histogram of the leakage current per detector area for Batch 1 (shown with cross hatch) and Batch 2. The leakage current was measured for the active area of the detector (i.e., guard ring currents were excluded) and was extrapolated [7] to the value at temperature 25°C. The leakage current per active area was specified to be less than 250 nA/cm² when the detector is biased at 10 V above its depletion voltage. The Batch 1 leakage currents are analyzed as a cluster around a single value, while Batch 2 leakage currents are analyzed as two distinct populations, those below 250 nA/cm² (Population 1), and those above it (Population 2). Table 2 summarizes leakage current information for the two batches. The systematic uncertainty in the measured value of leakage current for an individual detector is 0.2% for Batch 1 and 2-4% for Batch 2.

Table 2: Leakage Current Statistics

Data Set	Sample Size	Percentage of Sample with $I_{\text{leakage}} < 250 \text{ nA/cm}^2$	Average $I_{\text{leakage}}/\text{area}$ (nA/cm ²)
Batch 1	24	54	$249 \pm 124 \pm 1$
Batch 2, Pop. 1	6	100	$19.4 \pm 6.3 \pm 0.8$
Batch 2, Pop. 2	2	0	$631 \pm 40 \pm 25$

There is a clear correlation between the use of the Batch 2 passivation

process and low leakage current. We expect that the two Batch 2 detectors which failed the leakage current specification would have been eliminated prior to delivery of a normal production run, since leakage current is normally monitored. There is no evidence for correlation between leakage current and the presence of the double-metal structure.

DEPLETION VOLTAGE

The depletion voltage is determined from the inflection point in a log-log plot of bulk capacitance versus applied voltage. The specified value for $V_{\text{depletion}}$ was 45 ± 15 V.

Table 3 indicates the fraction of detectors in each batch which met the specification and the average depletion voltage for each batch. The central value of approximately 65 V is consistent with the choice of high resistivity silicon. The spread of values reflects the fact that wafers were fabricated from more than one ingot [3]. The dominant source of systematic error is the curve-fitting procedure used to derive $V_{\text{depletion}}$. We assign a value of 1.0 V to that error. Systematic errors associated with variations in temperature and humidity are both considerably less than this.

Table 3: Depletion Voltage Statistics

Batch	Percentage of Detectors with $30\text{V} \leq V_{\text{depletion}} \leq 60\text{V}$	Average $V_{\text{depletion}}$ (Volts)
Batch 1	25	$65 \pm 5 \pm 1$
Batch 2	37	$63 \pm 5 \pm 1$

We have investigated the dependence of depletion voltage upon the width-to-pitch ratio of the p - and n -side implants. A model [8] exists for the case where the implant pitches on the two detector sides are equal. One possible generalization of Reference 8's Equation 7 to the case of unequal p - and n -side pitches (p and p' , respectively) leads to the following expression for depletion voltage, V_D :

$$V_D = V_{D0} \left\{ 1 + 2 \frac{p}{d} \left[f \left(\frac{w}{p} \right) \right] + 2 \frac{p'}{d} \left[f \left(\frac{w'}{p'} \right) \right] \right\}, \quad (1)$$

where V_{D0} is the depletion voltage of a planar diode of the same active volume, electrical permittivity, and dopant concentration as the segmented detector in question, d is the detector thickness, w and w' are the widths of the implants on the p - and n -sides, respectively, and f is the function defined in Reference 8 to account for the non-parallel nature of the electric field lines in the vicinity of the detector's strips. We denote the expression enclosed by braces in Equation 1 as the " p - and n -side segmentation correction factor," $F_{p,n}$.

Our data suggest that the term in the segmentation correction factor that reflects the n -side structure is not optimized. In fact, the analysis below indicates that depletion voltage data for detectors segmented *on both sides* are actually better described by a version of Equation 1 in which only the p -side structure is reflected:

$$V_D = V_{D0} \left\{ 1 + 2 \frac{p}{d} \left[f \left(\frac{w}{p} \right) \right] \right\}. \quad (2)$$

We denote the expression enclosed by braces in Equation 2 as the " p -side segmentation correction factor," F_p .

We can test which of Equations 1 and 2 better describes the effect of n -side segmentation upon depletion voltage as follows. If fringing effects are neglected, the value of V_{D0} depends solely upon the effective charge carrier density $N_{\text{effective}}$, thickness d , and permittivity ϵ_{Si} of the bulk silicon,

$$V_{D0} = \frac{qd^2 |N_{\text{effective}}|}{2\epsilon_{\text{Si}}}, \quad (3)$$

where q is the absolute value of the electron charge. Consequently, we expect the ratio of the average measured depletion voltage, $\langle V_D \rangle$, for each detector type, to the appropriate segmentation correction factor for that type, to be a constant for detector types A, B, C, and D (which provide a variety of ratios of width-to-pitch for both detector sides).

Figure 2 is a histogram of the depletion voltages that were measured for the SINTEF/SI detectors. Since no correlation was found between depletion voltage and batch number, the 32 detectors are treated as a single data set. Each entry in the histogram is patterned to indicate the type (A, B, C, or D) of detector that was measured. Column 2 of Table 4 lists $\langle V_D \rangle$ for each detector type. Columns 3 and 4 list the values of F_p and $F_{p,n}$,

respectively, for each detector type, as they are calculated from that type's widths, pitches, thickness, and function f . (The functional form of f is given in Figure 8 of Reference 8). Columns 5 and 6 show the ratio of $\langle V_D \rangle$ to each of the correction factors.

We use the Particle Data Group method [9] for unconstrained averaging to examine the self-consistency of the entries in Columns 5 and 6 as follows. We make the conservative assumption that the systematic errors quoted in these two columns are completely correlated. We then calculate a χ^2 for the four entries in each column, taking the statistical error alone as the uncertainty on each value. We find that the χ^2 for the entries in Column 5 is 12, while that for the entries in Column 6 is 164. Since in both cases the number of degrees of freedom is 4, we conclude that, while neither F_p nor $F_{p,n}$ is completely adequate as a correction for double-sided detector segmentation, the values given by $\langle V_D \rangle / F_p$ are in significantly better agreement than are those given by $\langle V_D \rangle / F_{p,n}$.

Table 4: Comparison of Segmentation Correction Factors

Type	Average Measured $V_{\text{depletion}} \langle V_D \rangle$	p -side Segmentation Correction Factor, F_p	p - and n -side Segmentation Correction Factor, $F_{p,n}$	$\langle V_D \rangle / F_p$	$\langle V_D \rangle / F_{p,n}$
A	$61 \pm 1 \pm 1$	1.03	1.46	$60 \pm 1 \pm 1$	$42 \pm 1 \pm 1$
B	$63 \pm 2 \pm 1$	1.13	1.56	$55 \pm 1 \pm 1$	$40 \pm 1 \pm 1$
C	$71 \pm 2 \pm 1$	1.13	1.40	$63 \pm 1 \pm 1$	$50 \pm 1 \pm 1$
D	$65 \pm 1 \pm 1$	1.13	2.00	$57 \pm 1 \pm 1$	$32 \pm 1 \pm 1$

BIAS RESISTANCE

All of the prototype detectors have polysilicon biasing resistors on both sides. Figure 3 is a histogram of the average bias resistance of each detector's n -side, for Batch 1 (cross hatched) and Batch 2. Figure 4 contains similar information for the p -side bias resistors. The values reported in Figures 3 and 4 are based upon measurement of five resistors on each side of each detector. The value of R_{bias} was specified to be $2.0\text{M}\Omega \pm 1.0\text{M}\Omega$.

Column 3 of Table 5 shows the percentage of detectors whose average

bias resistance meets the specification. Column 4 shows the average R_{bias} for the batch. The uncertainties quoted in Column 4 represent the statistical errors in central values for all detectors in each batch. The uncertainty on the resistance of any particular bias resistor is less than 1%. The uncertainty on the mean bias resistance per side of a typical detector is 5%. Temperature variations between 22°C and 32°C and relative humidity variations between 21% and 67% were found to contribute uncertainty of less than 0.2% to the resistance obtained for any particular resistor.

Table 5: Bias Resistance Statistics

Batch	Side	Percentage of Detectors with $1\text{M}\Omega \leq R_{\text{bias}} \leq 3\text{M}\Omega$	Average R_{bias} (M Ω)
Batch 1	<i>n</i> -side	0	$5.27 \pm 3.47 \pm 0.05$
Batch 2	<i>n</i> -side	0	$22.7 \pm 8.60 \pm 0.23$
Batch 1	<i>p</i> -side	79	$1.26 \pm 0.63 \pm 0.01$
Batch 2	<i>p</i> -side	63	$1.02 \pm 0.41 \pm 0.01$

The statistical error on the mean value of the Batch 1 *n*-side bias resistance is highly influenced by the contributions from the two detectors with $R_{\text{bias}} > 16 \text{ M}\Omega$. If those two detectors are removed from the sample, the standard deviation for the Batch 1 *n*-side resistors reduces from 3.47 M Ω to 0.60 M Ω .

The short, or A- and B-type, detectors were fabricated on the outer portion of the wafer, while the long, or C- and D-type, detectors were fabricated from the wafer's center. No systematic variation of R_{bias} with position on the wafer is observed.

The *p*-side bias resistances show a high yield for both Batch 1 and Batch 2. The systematically high value of the *n*-side Batch 1 bias resistances (relative to the specified value of $2.0\text{M}\Omega \pm 1.0\text{M}\Omega$) is directly traceable to a mask error which would have been corrected in a production run [3]. The *n*-side bias resistance for the Batch 2 detectors is much larger than expected. To confirm that our reported value was correctly measured with the techniques described in Reference 5, test structures supplied by the manufacturer were examined. The isolated bias resistors on the test structures were measured with an ohmmeter and found to have resistances consistent with the value

reported in Table 5.

INTERSTRIP RESISTANCE

The specified minimum resistance between implant strips, $R_{\text{interstrip}}$, was 500 M Ω .

Figure 5 shows the average $R_{\text{interstrip}}$ for the n -side of Batch 1 detectors. One Batch 1 detector drew high current during the measurement of its n -side which prevented a reliable value of $R_{\text{interstrip}}$ from being obtained. One other detector was found to have an n -side interstrip resistance of 225 ± 12 G Ω ; to improve the readability of Figure 5, we do not include that entry. (It is, however, included in all of the statistical calculations). Due to an effect described below, only one of the Batch 2 detectors was able to have its n -side $R_{\text{interstrip}}$ value measured. Figure 6 shows the average $R_{\text{interstrip}}$ for the p -sides of Batch 1 (cross hatched) and Batch 2 detectors. The error on the central value obtained for each detector's interstrip resistance is 1%.

Figures 5 and 6 show that both batches' detectors form two populations when classified by interstrip resistance. We label as " n -side Population 1" the two Batch 1 detectors with n -side interstrip resistance greater than 20 G Ω . We label as " p -side Population 1" the three Batch 1 and one Batch 2 detectors with p -side interstrip resistance greater than 100 M Ω . The remainder of the detectors are classified as "Population 2."

We summarize here the procedure used to measure interstrip resistance, as it is described in Reference 5. The procedure utilizes the fact that the bias trace is divided into two parts. Each part is connected to one-half of the implants, and the two groups of implants are interleaved. This arrangement permits the experimenter to apply a voltage between neighboring implants and determine $R_{\text{interstrip}}$ by recording the current induced between the implants as a function of the size of the potential difference. Correction is made for current flow through the bias resistors. No correction is made for current flow from strips to the guard ring, as that is expected to be negligible in a properly functioning detector.

During the n -side interstrip resistance measurement of the Batch 2 detectors, two effects were observed that were not present in Batch 1 detectors. The first effect is the fact that the uncertainty associated with the strip cur-

rents on the n -side of Batch 2 detectors is much larger than it is for currents measured on Batch 1 or the p -side of Batch 2 detectors. To ensure that the effect is not due to measurement error, Batch 1 and Batch 2 detectors are measured together. The Batch 1 detectors consistently produce leakage currents whose values are reproducible to within 0.2%. Each Batch 2 detector was measured several times, with consistently larger leakage current uncertainty of 2-4%. The primary source of systematic error in the Batch 2 n -side interstrip resistance values is the error in the currents.

The second effect observed in the Batch 2 detectors is low isolation between n -side implant strips and the guard ring relative to Batch 1. This poses a fundamental problem for measurement of the interstrip resistance, because the technique for measuring interstrip resistance presumes that when the differential voltage is applied between the two groups of interleaved implants, leakage current collected on the strips at higher potential will increase linearly with potential difference, with negligible current collection on the guard ring. With Batch 1 detectors, that is what happens, despite the fact that the guard ring is located between the bias ring and the strips. With Batch 2 detectors, a significant amount of current is collected on the guard ring when a differential voltage is applied between groups of implants. The loss of interstrip current to the guard ring prevents a reliable measurement of interstrip resistance by the techniques in Reference 5. One of the Batch 2 detectors does not exhibit this effect; its n -side interstrip resistance value is $133 \pm 5 \text{ G}\Omega$ (statistical error only).

Column 3 of Table 6 indicates the fraction of detectors whose average $R_{\text{interstrip}}$ meets specification. None of the detectors have a value of $R_{\text{interstrip}} > 500 \text{ M}\Omega$ for their p -side. The cause of this failure remains under investigation. Most of the Batch 1 detectors and the measurable Batch 2 detector have n -side $R_{\text{interstrip}}$ values that exceed $500 \text{ M}\Omega$.

Systematic errors due to variations in temperature and humidity are no larger than 0.8% and 1.0%, respectively. We observed no correlation between interstrip resistance and the presence of the double-metal structure.

Table 6: Interstrip Resistance Statistics

Data Set	Side	Fraction of Detectors with $R_{\text{interstrip}} \geq 500\text{M}\Omega$	Average $R_{\text{interstrip}}$ ($\text{M}\Omega$)
Batch 1, Pop. 1	<i>n</i> -side	2/2	$134000 \pm 128000 \pm 1720$
Batch 1, Pop. 2	<i>n</i> -side	18/21	$4280 \pm 400 \pm 55$
Batch 1, Pop. 1	<i>p</i> -side	0/3	$241 \pm 133 \pm 3$
Batch 1, Pop. 2	<i>p</i> -side	0/21	$20.1 \pm 12.9 \pm 0.3$
Batch 2, Pop. 1	<i>p</i> -side	0/1	$347 \pm 1 \pm 4$
Batch 2, Pop. 2	<i>p</i> -side	0/7	$25.2 \pm 20.8 \pm 0.4$

COUPLING CAPACITANCE

The coupling capacitance, C_{coupling} , was specified to be at least 7 times larger than the capacitance with respect to neighboring strips. Measurements [4] of the capacitance with respect to neighboring strips suggest that it is less than 1 pF/cm for these detectors. The coupling capacitors meet their specification.

Five coupling capacitors were measured on each side of every SINTEF/SI SVXII prototype detector. Figure 7 shows the average coupling capacitance per implant length for the *n*-sides of Batch 1 (cross hatched) and Batch 2 detectors. Figure 8 shows the same information for the *p*-sides.

Table 7 shows the average C_{coupling} per unit length of implant. The errors quoted are statistical only. The systematic uncertainty associated with the measurement of each *n*-side coupling capacitor is 5%. The systematic error associated with *p*-side capacitor measurements remains under investigation [4]. The detectors are grouped by location on the wafer; as mentioned above, types A and B were fabricated near the edge, while types C and D were fabricated near the center. We observe no evidence for variation in coupling capacitance as a function of position of the capacitor on the wafer.

Table 7: Coupling Capacitor Statistics

Type		A and B	C and D
Batch	Side	$C_{\text{coupling}}/\text{length}$ (pF/cm)	$C_{\text{coupling}}/\text{length}$ (pF/cm)
Batch 1	<i>n</i> -side	21 ± 2	22 ± 4
Batch 2	<i>n</i> -side	22 ± 2	24 ± 2
Batch 1	<i>p</i> -side	17 ± 7	18 ± 11
Batch 2	<i>p</i> -side	17 ± 6	15 ± 7

COUPLING CAPACITOR BREAKDOWN VOLTAGE

The coupling capacitors are required to operate stably with an applied potential up to 120V. This high value may be needed in order for the detectors to operate after irradiation.

A total of 1008 capacitors on Batch 1 detectors were characterized by having 120V applied across them. No channel tested in this way showed more than 0.1 nA across its dielectric.

A total of 78 capacitors on Batch 2 detectors were similarly studied. Of these, 76% failed to withstand 120V. The reduced robustness of the Batch 2 capacitors is thought to be due to lack of registration between the masks used to fabricate the capacitors' silicon nitride and silicon dioxide layers [3]. This registration failure would have been corrected in a production run.

3 ACKNOWLEDGEMENTS

We thank Anders Hanneborg and Lars Evensen of SINTEF/SI for providing valuable information about wafer processing and characterization.

References

- [1] Bacchetta, N., et al., *SVX II Simulation and Upgrade Proposal*, CDF Collaboration Note CDF/DOC/SEC_VTX/CDFR/1922 (January

- 1993).
- [2] Seidel, S., *Specifications for SVX II Double-Metal Microstrip Detector Prototypes*, CDF Collaboration Note CDF/DOC/SEC_VTX/CDFR-/2030 (May 1993).
 - [3] Hanneborg, A., SINTEF/SI, private communication.
 - [4] Frautschi, M.A., et al., *Capacitance Measurements of Double-sided Silicon Microstrip Detectors*, CDF Collaboration Note CDF/DOC/SEC_VTX/CDFR/2546, submitted to *Nucl. Instr. and Meth. in Phys. Res.*
 - [5] Bruner, N.L., et al., *Characterization Procedures for Double-Sided, Double-Metal Silicon Microstrip Detectors*, *Nucl. Instr. and Meth. in Phys. Res., A* **362** pp. 315-337 (1995).
 - [6] Patton, A., et al., *Electrical Characterization of SINTEF/SI SVX II Prototype Double-sided Silicon Microstrip Detectors*, CDF Collaboration Note CDF/DOC/SEC_VTX/CDFR/2835 (June 1995).
 - [7] Barberis, E., et al., *Nucl. Instr. and Meth. in Phys. Res. A* **326** pp. 373-380 (1993).
 - [8] Barbaris, E., et al., *Nucl. Instr. and Meth. in Phys. Res. A* **342** pp. 90-95 (1994).
 - [9] Particle Data Group, *Phys. Rev. D* **50** p. 1180 (1994).

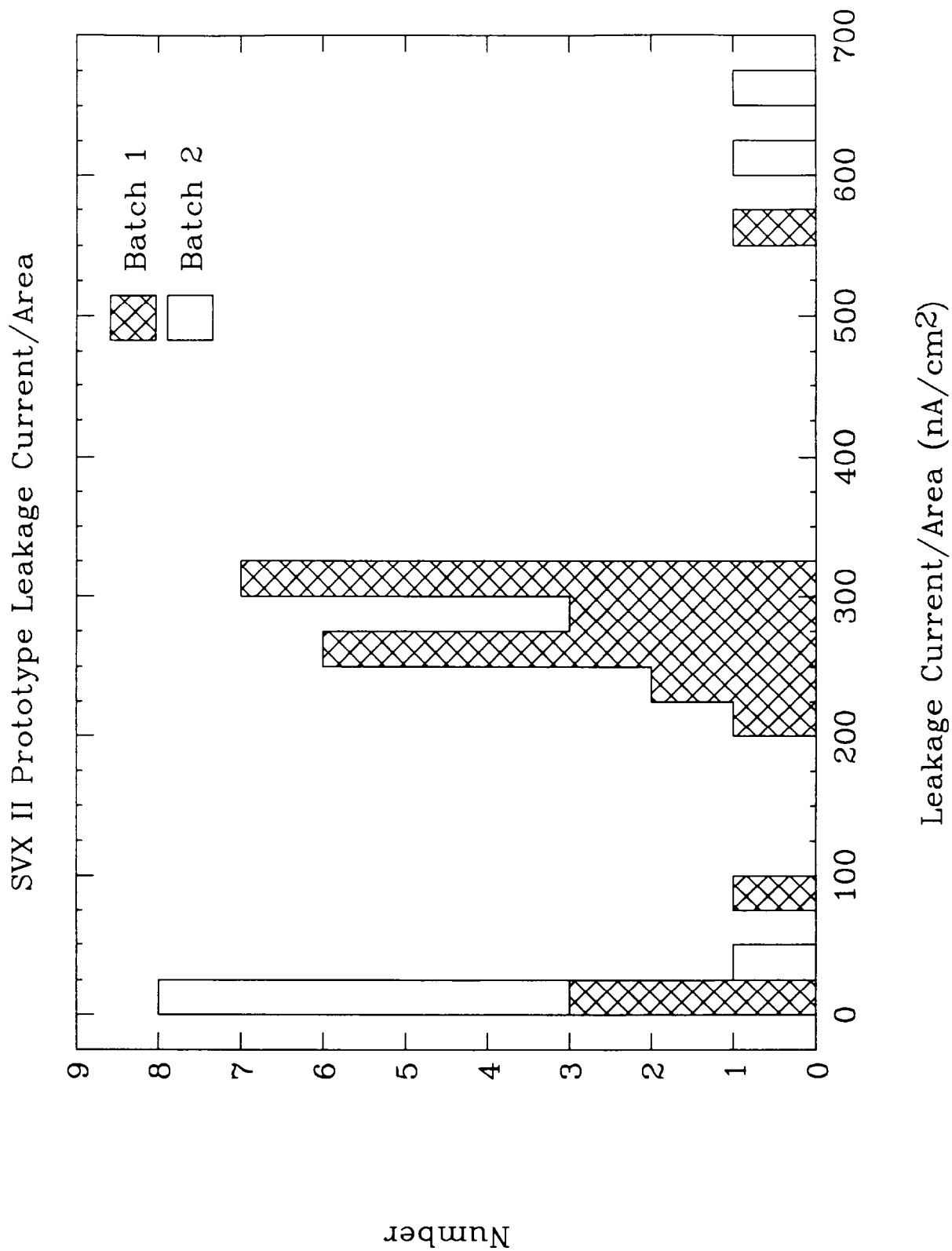
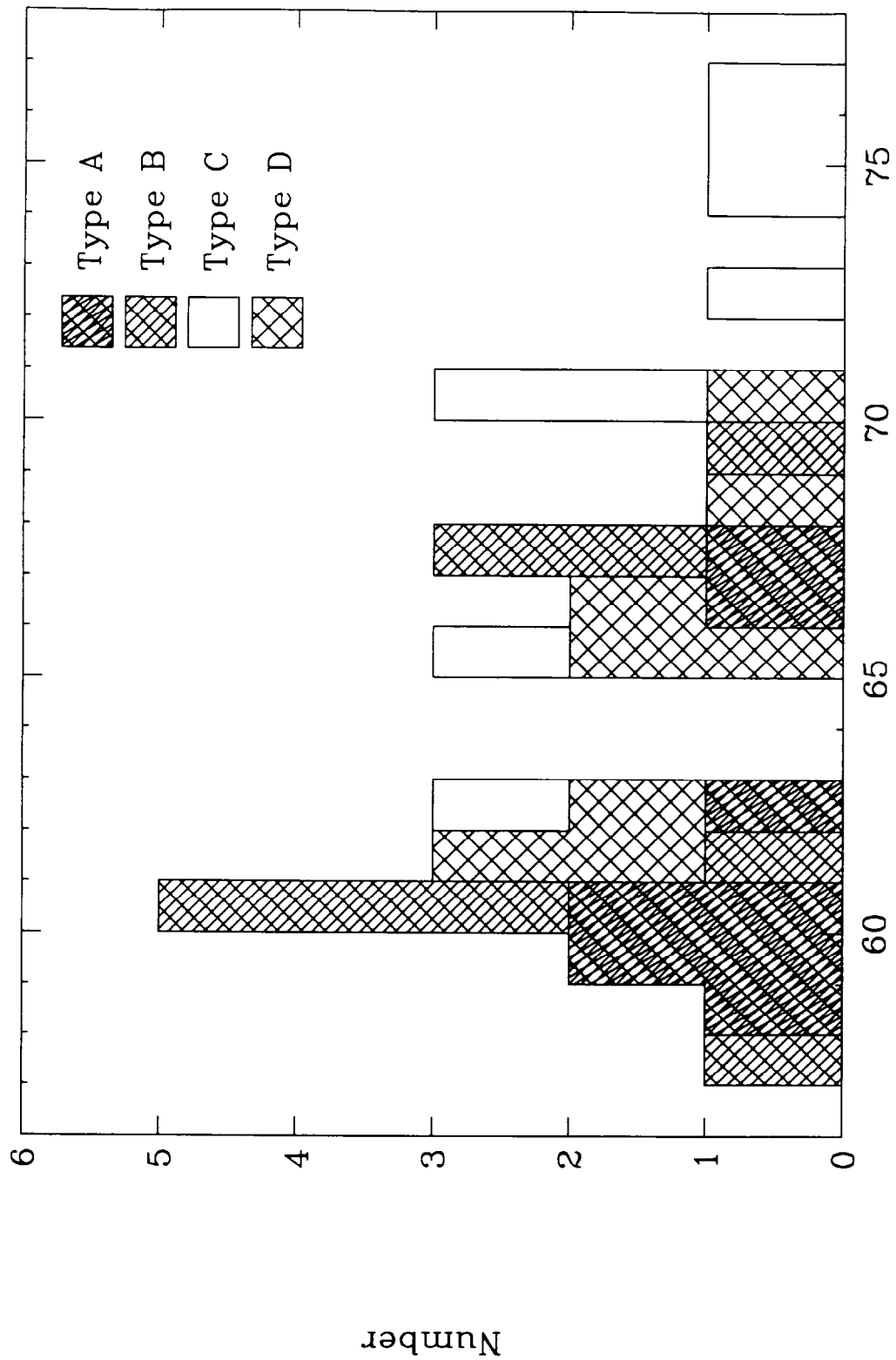


Figure 1: Leakage current per active area of SINTEF/SI SVX II prototype detectors.

SVX II Prototype Depletion Voltage



Depletion Voltage (Volts)

Figure 2: Depletion voltage of SINTEF/SI SVX II prototype detectors.

SVX II Prototype n-side Bias Resistance

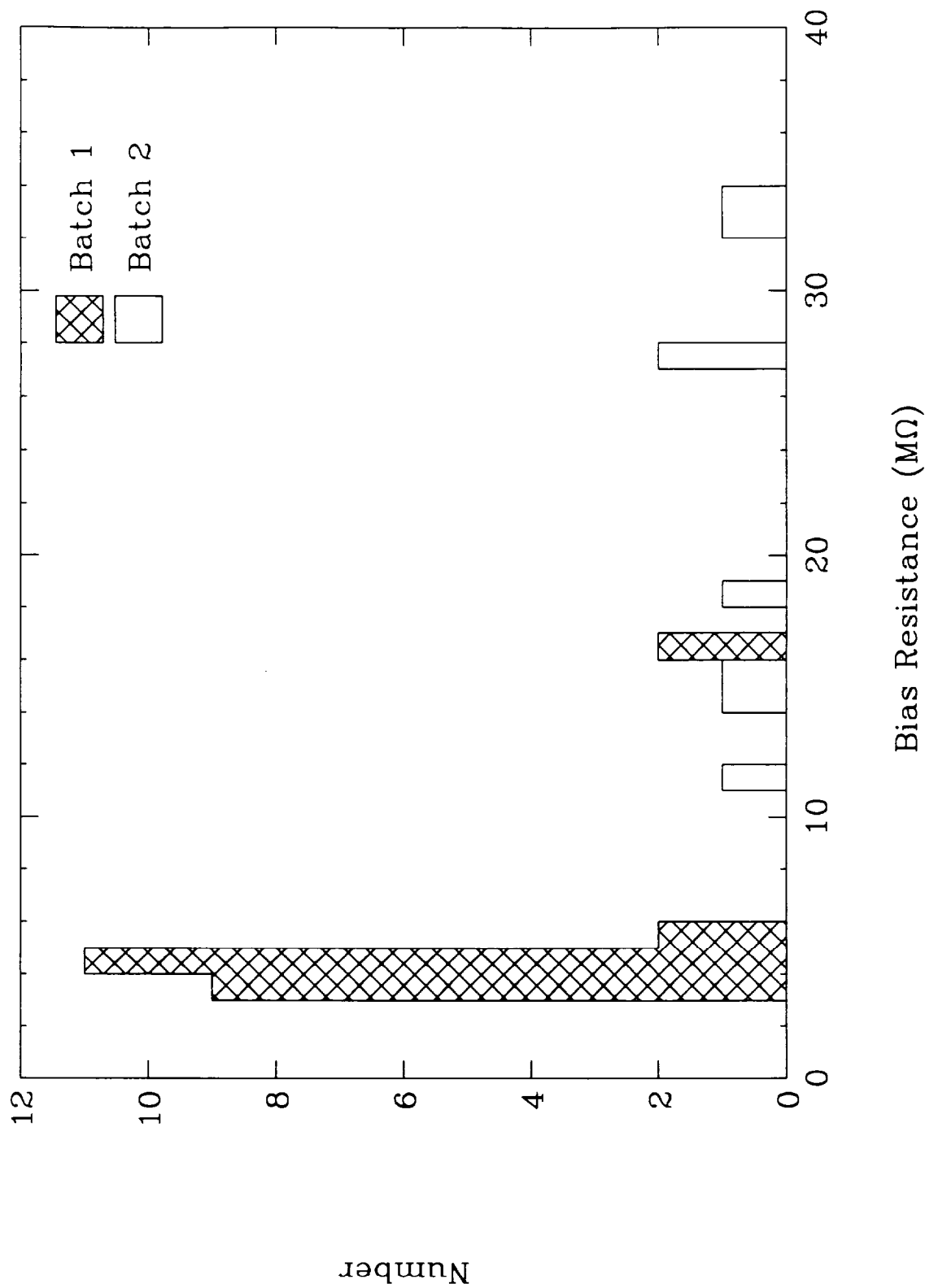


Figure 3: Resistance of *n*-side polysilicon bias resistors on SINTEF/SI SVX II prototype detectors.

SVX II Prototype p-side Bias Resistance

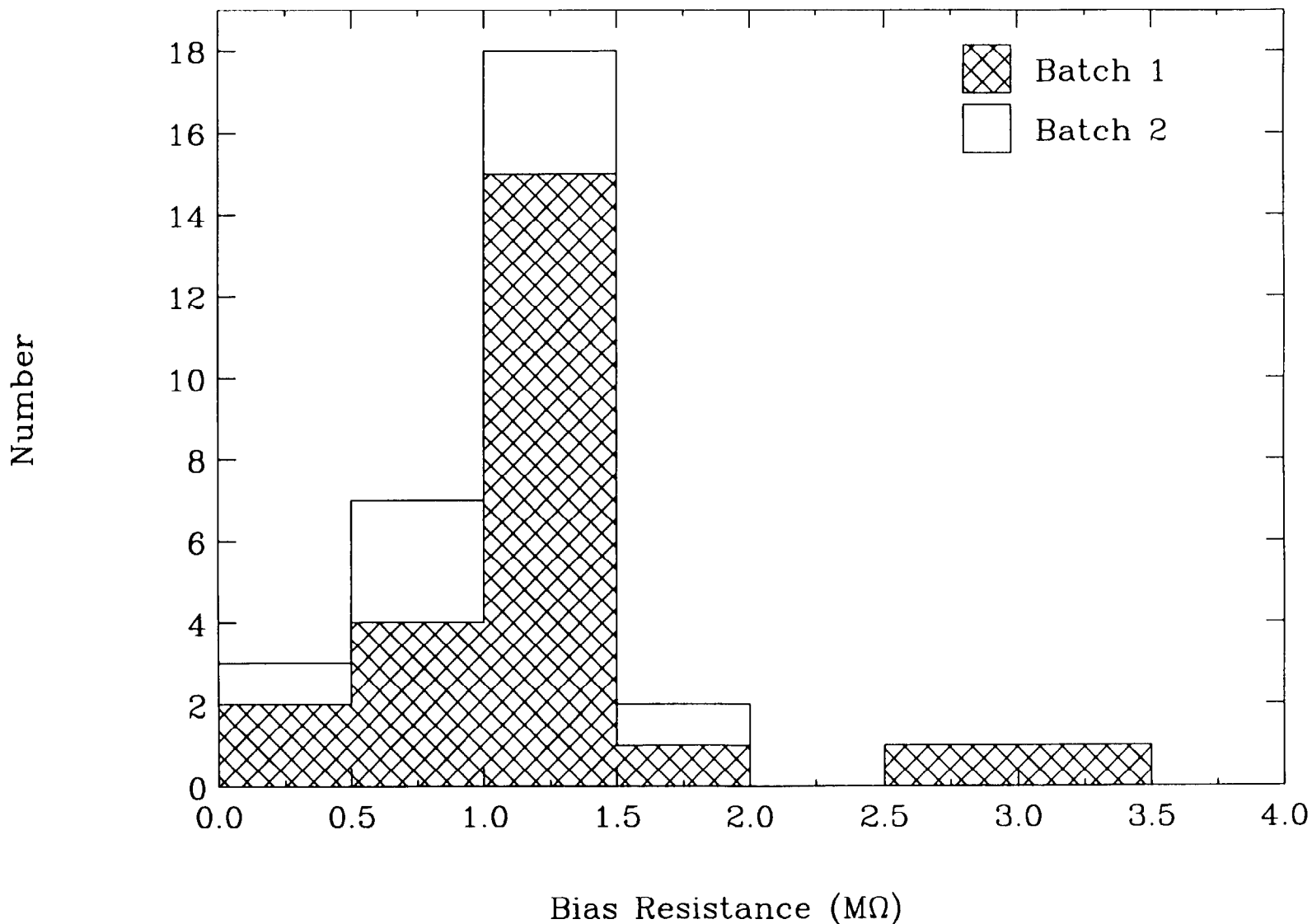


Figure 4: Resistance of *p*-side polysilicon bias resistors on SINTEF/SI SVX II prototype detectors.

SVX II Prototype n-side Interstrip Resistance

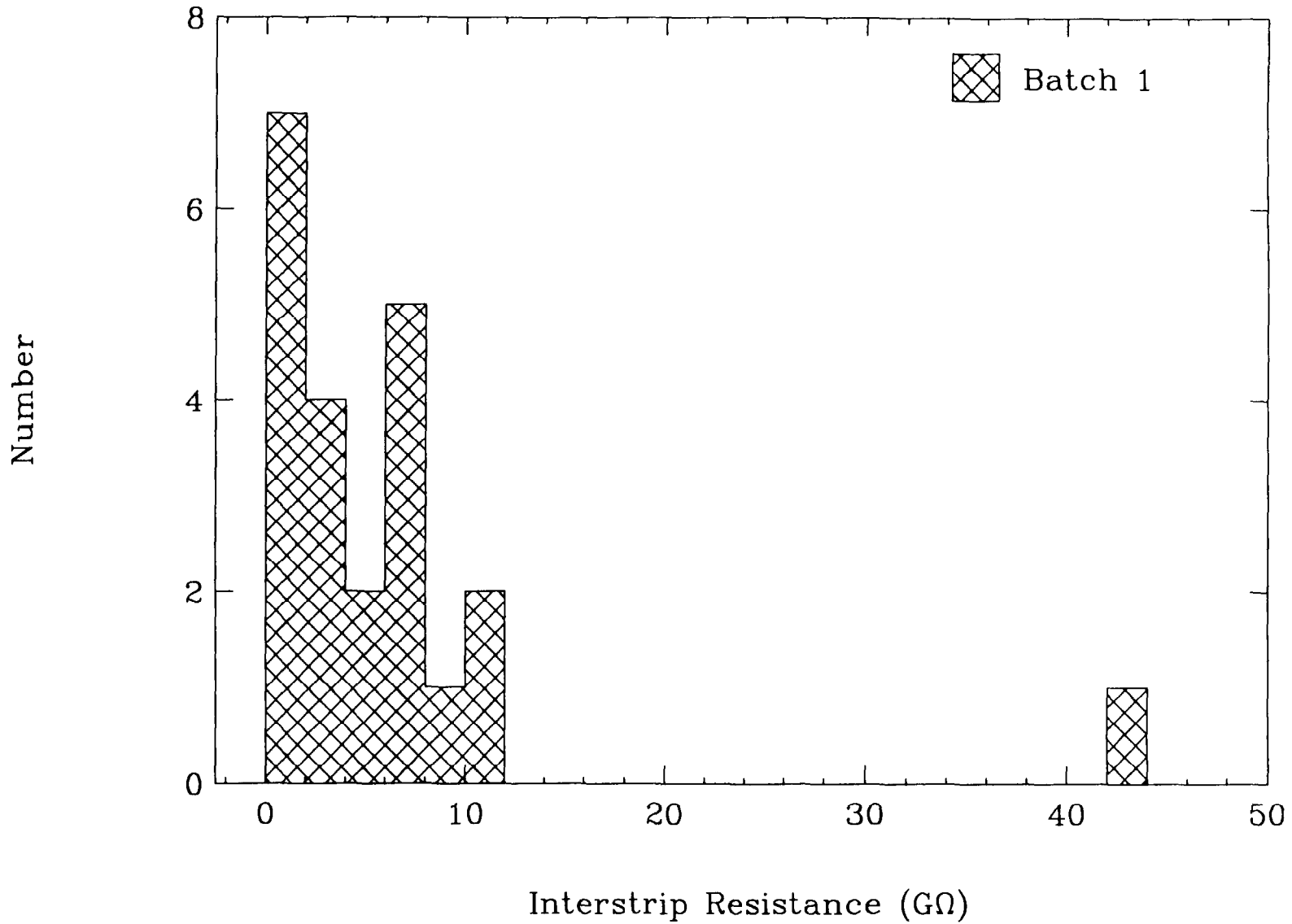


Figure 5: Interstrip resistance on the *n*-side of SINTEF/SI SVX II prototype detectors.

SVX II Prototype p-side Interstrip Resistance

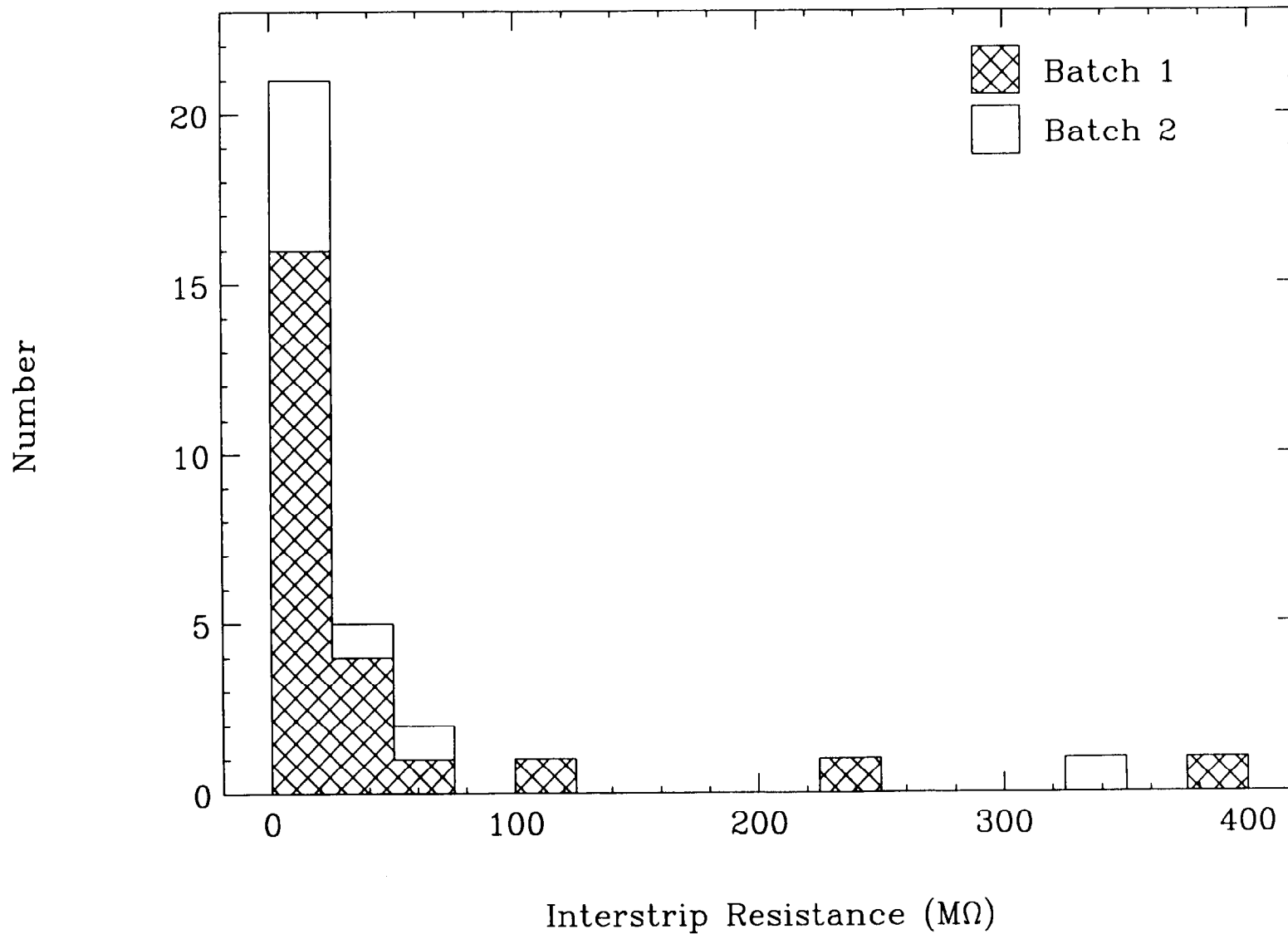


Figure 6: Interstrip resistance on the *p*-side of SINTEF/SI SVX II prototype detectors.

SVX II Prototype n-side Coupling Capacitance per Length

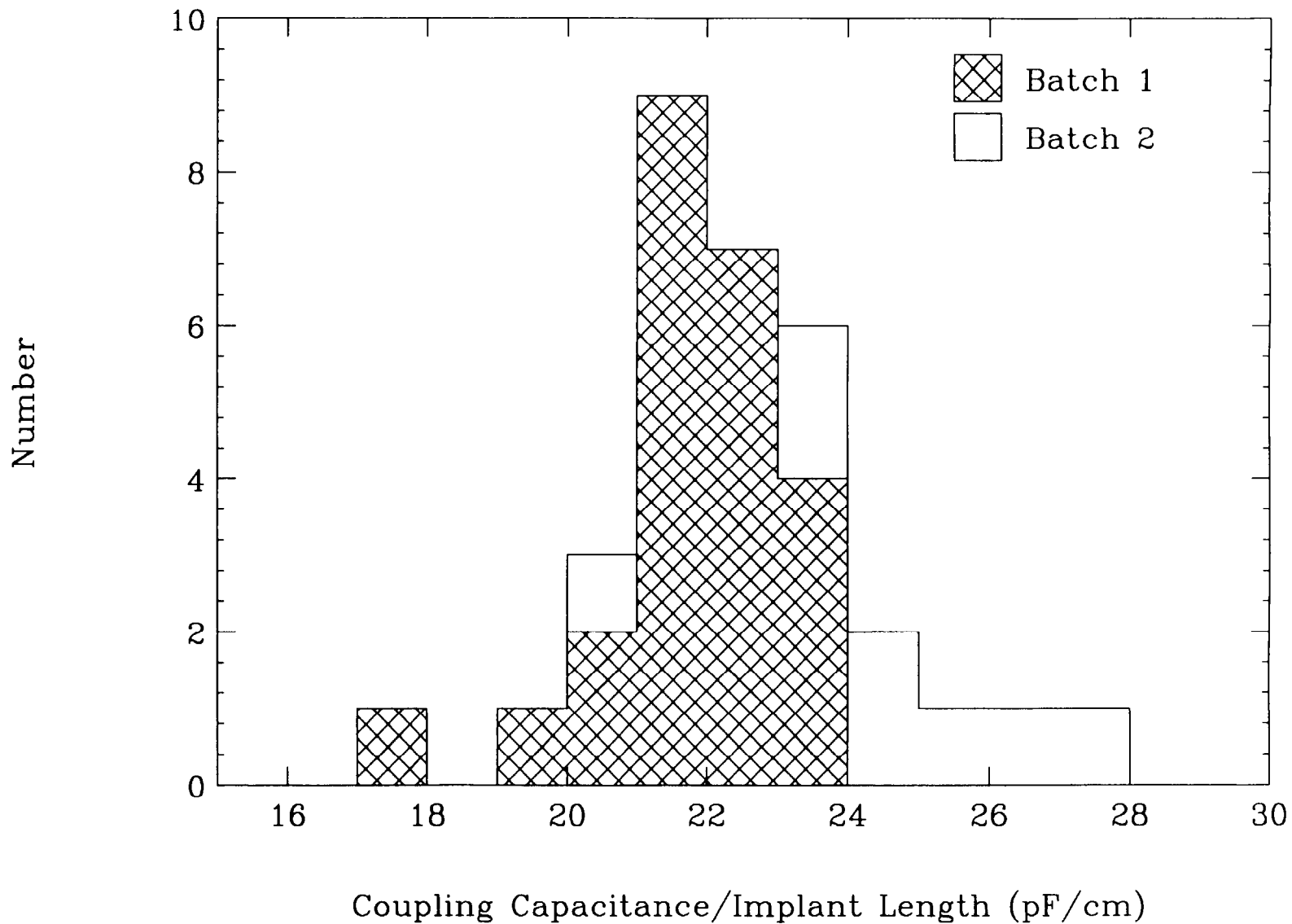


Figure 7: Capacitance per length of coupling capacitors on the *n*-side of SINTEF/SI SVX II prototype detectors.

SVX II Prototype p-side Coupling Capacitance per Length

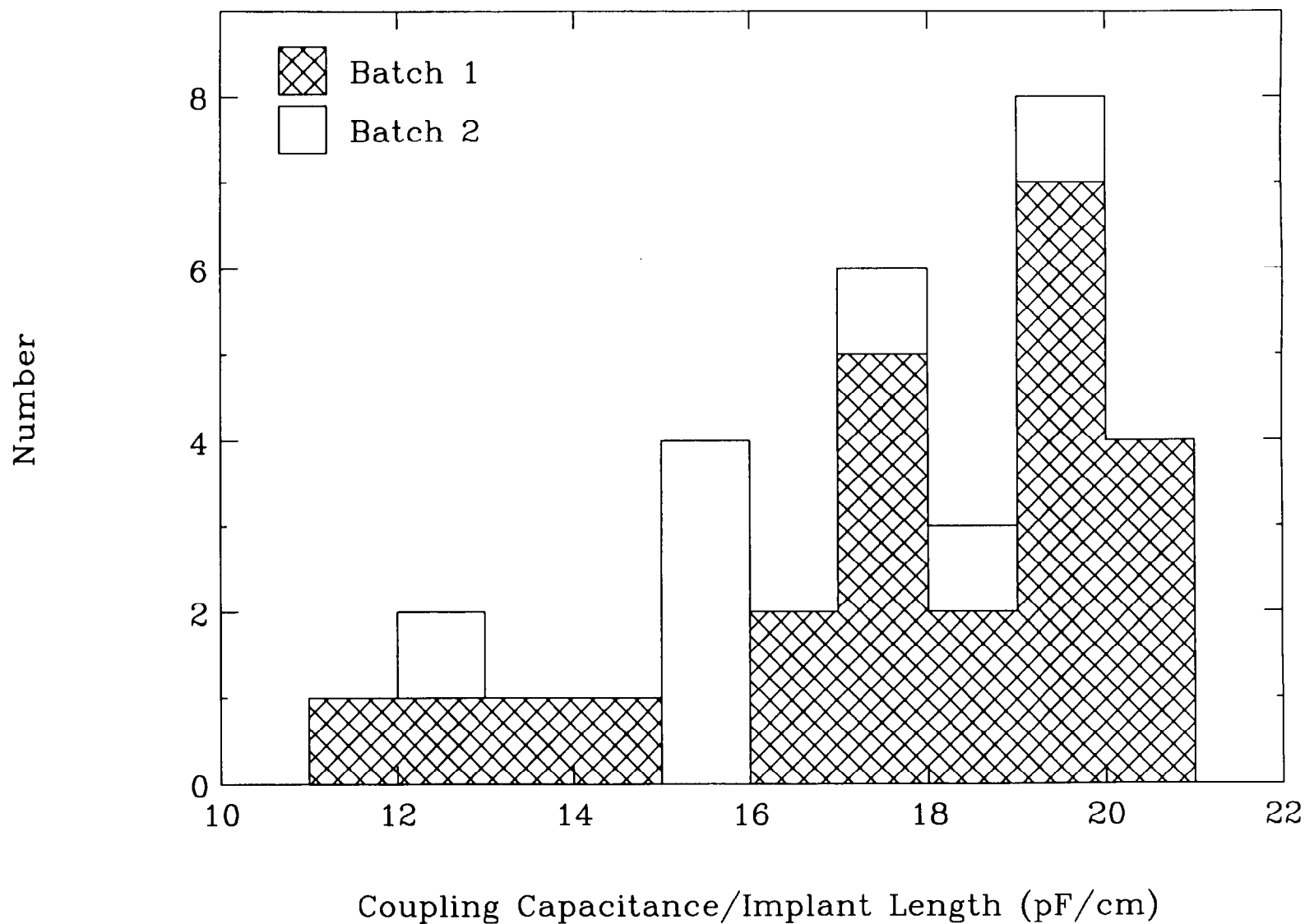


Figure 8: Capacitance per length of coupling capacitors on the *p*-side of SINTEF/SI SVX II prototype detectors.